Available online at www.sciencedirect.com
ScienceDirect
J. Mater. Sci. Technol., 2012, **28**(11), 1031–1038.
JMST
www.JMST.org

Microstructure of Carbides at Grain Boundaries in Nickel Based Superalloys

Xiaoming Dong[1)], *Xiaoli Zhang*[2)], *Kui Du*[1)†], *Yizhou Zhou*[2)], *Tao Jin*[2)] *and Hengqiang Ye*[1)]
1) Shenyang National Laboratory for Materials Science, Institute of Metal Research, Chinese Academy of Sciences, Shenyang 110016, China
2) Institute of Metal Research, Chinese Academy of Sciences, Shenyang 110016, China
[Manuscript received April 17, 2012, in revised form July 9, 2012]

It is well known that carbides at grain boundaries play an important role in affecting mechanical properties of nickel based superalloys. In order to deeply understand the relationship between grain boundary structures and properties, in this work, we have investigated the microstructure of grain boundaries with different misorientation angles in bicrystals of nickel based superalloys. It is found that the bicrystals with smaller misorientation angles contain denser $M_{23}C_6$ but sparse MC particles at grain boundaries, and this kind of bicrystals presents longer stress rupture lives. It was observed that MC carbides were decorated by $M_{23}C_6$ and M_6C particles at grain boundaries. The formation of these carbide particles, therefore, is likely due to the local fluctuation of chemical composition around MC carbides. In addition, the orientation relationships between MC carbides and $\gamma/\gamma\prime$ matrix were also determined.

KEY WORDS: **Electron microscopy; Ni based superalloys; Grain boundaries; Orientation relationship**

1. Introduction

Nickel based superalloys are widely employed for turbine blades because of their excellent creep and fatigue strengths, particularly, in the form of single crystal. Due to the complex shape of the blades, however, it is hard to avoid the formation of grain boundaries during casting process for single crystal blades[1]. The presence of grain boundaries leads to component rejection, and is therefore, seriously deleterious to mechanical properties of the blades[2]. In practice, carbides and borides are commonly utilized to strengthen grain boundaries and consequently improve the mechanical properties of nickel based superalloy blades. Eutectic MC carbides as well as $M_{23}C_6$ particles at grain boundaries often inhibit grain boundary migration during deformation, thus enhance the fatigue performance of superalloys[3–5]. Besides, fine and dispersive M_6C particles can pin down dislocation movement, prevent γ' phase to be sheared and thus strengthen the superalloy[5,6]. However, continuous carbide chains formed at grain boundaries would facilitate the initiation and propagation of cracks resulting in the failure of superalloys[7]. It is because of the above-mentioned complex and significant effects of carbides on mechanical properties of superalloys, now researches are of great interest on the morphology, formation mechanism of carbides at grain boundaries, especially when the morphology, size, distribution and stability of carbides vary with superalloy composition and fabrication processes[2,8,9]. This work investigated the variation of the rupture life and the microstructure of grain boundaries in bicrystals of Ni based superalloys. Additionally, the orientation relationships (ORs) between MC carbides and γ/γ' matrix were also determined by electron diffraction.

† Corresponding author. Prof., Ph.D.; Tel.: +86 24 83970725; Fax: +86 24 23891320, E-mail address: kuidu@imr.ac.cn (K. Du).

2. Experimental

Table 1 presents the chemical composition of the superalloy based on a SRR99 alloy studied in this work. To study the microstructure of grain boundaries, bicrystal plates were cast by means of a seeding technique in a directional solidification vacuum furnace. Both [001] directions in the seeds were parallel to the directional solidification direction. The [100] direction in one seed was parallel to a given reference plane. The [100] direction in the other seed was rotated along its [001] direction making a predefined angle between the [100] direction and the reference plane. By using such seeding technique, the bicrystal plates containing the grain boundaries with different tilt angles were obtained. In this work, each sample was cut to contain one tilt grain boundary. The misorientation angles of the studied bicrystal samples were determined as 4°, 8° and 13° by the electron backscatter diffraction (EBSD) in the scanning electron microscope (SEM). The plates were then solution treated at 1300 °C for 4 h followed by aging treatment of 4 h at 1100 °C and 16 h at 870 °C for further investigating the microstructure variation in them.

Table 1 Chemical composition of the studied superalloy (wt%)

Al	Co	Cr	Ta	Ti	W	C	Ni
5.5	5	8.0	3	2.2	10	0.015	Bal.

The specimens used for stress rupture tests were selected from the heat treated plates and machined along the solidification direction. The rupture tests were carried out at 800 °C and under a stress of 750 MPa with the principal loading axis perpendicular to the grain boundaries. The cross-section electron microscopy samples were selected from the heat treated bicrystal plates and prepared. The microstructure of the samples was studied using the Tecnai F30 scanning transmission electron microscope (STEM), Tecnai F20 transmission electron microscope (TEM) and JSM-6301F field emission SEM. The TEM specimens were prepared by conventional cutting, grinding and ion-milling, the SEM specimens were polished and etched in a solution of 40 ml C_2H_5OH, 1.5 g $CuSO_4$ and 20 ml H_2O. In this work, the high-angle annular dark-field (HAADF) detector was used for Z-contrast imaging and the X-ray energy dispersive spectrometer (EDS) for microanalysis, which are equipped in the STEM.

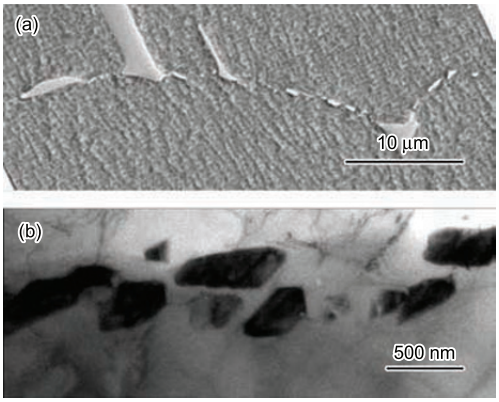

Fig. 1 SEM (a) and TEM (b) micrographs of carbides at grain boundaries

3. Results

3.1 Microstructure and stress rupture life of bicrystal superalloys

It is experimentally found that, while cubic γ' precipitates are embedded in γ phase matrix, carbides are prominently located at grain boundaries in superalloys. In this work, the chemical compositions and crystal structures of carbides were identified by EDS analysis combining with electron diffraction, their lattice parameters were determined by electron diffraction and shown in Table 2. Three types of carbides, MC, M_6C and $M_{23}C_6$, were determined at grain boundaries. MC carbides are Ta and Ti-rich and mostly present in the blocky or needle-like form. These carbides are large and distribute sparsely well at grain boundaries (Fig. 1). In addition, small amounts of filmated MC were found in some parts of the grain boundaries. It is found that the carbides at grain boundaries are mainly composed of blocky W, Ni and Cr-rich M_6C particles and they are considerably smaller than blocky MC carbides. There exist finer $M_{23}C_6$ particles at grain boundaries as well as in γ channels in the matrix. At the cross of two γ channels, however, the precipitated $M_{23}C_6$ particles are commonly larger than those inside γ channels (Fig. 2). Fig. 3(a) shows the size distribution of carbides along

Table 2 Chemical compositions, space groups and lattice parameters of different phases in the superalloy. a is the lattice parameter of a crystal

	Chemical composition/at.%							Space group	a /nm
	Al	Ti	Cr	Co	Ni	Ta	W		
γ	2.61	0.34	26.10	10.18	54.31	1.22	5.23	$Fm3m$	0.366 ± 0.007
γ'	10.26	3.51	2.68	3.57	71.41	3.23	5.34	$Pm3m$	0.363 ± 0.007
MC	1.30	45.15	1.53	0.06	3.82	41.58	6.55	$Fm3m$	0.448 ± 0.009
M_6C	1.95	2.47	21.65	6.91	26.24	3.30	37.49	$Fd3m$	1.145 ± 0.023
$M_{23}C_6$	0.51	0.88	79.70	1.50	7.04	1.14	9.23	$Fm3m$	1.112 ± 0.022

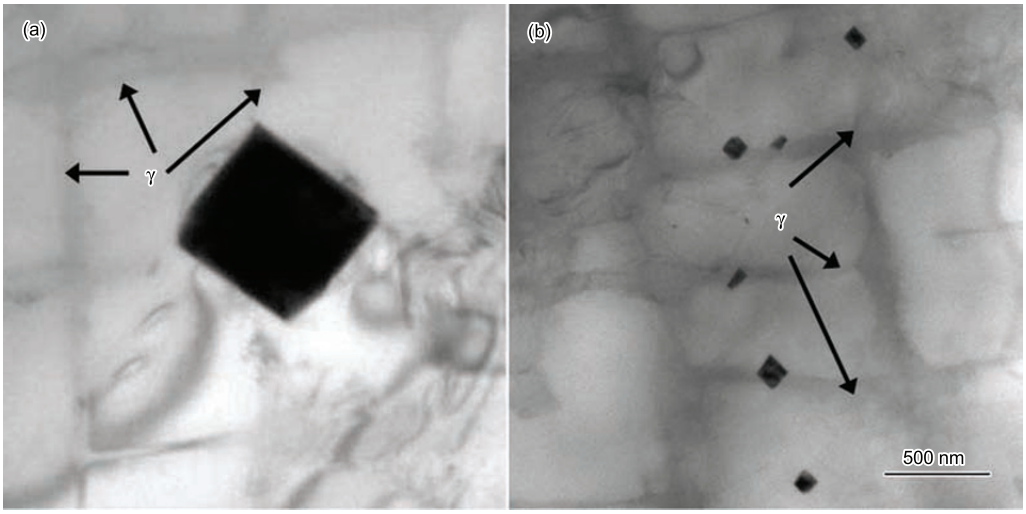

Fig. 2 $M_{23}C_6$ particles (dark contrast) in a cross of two γ channels (a) and inside γ channels (b)

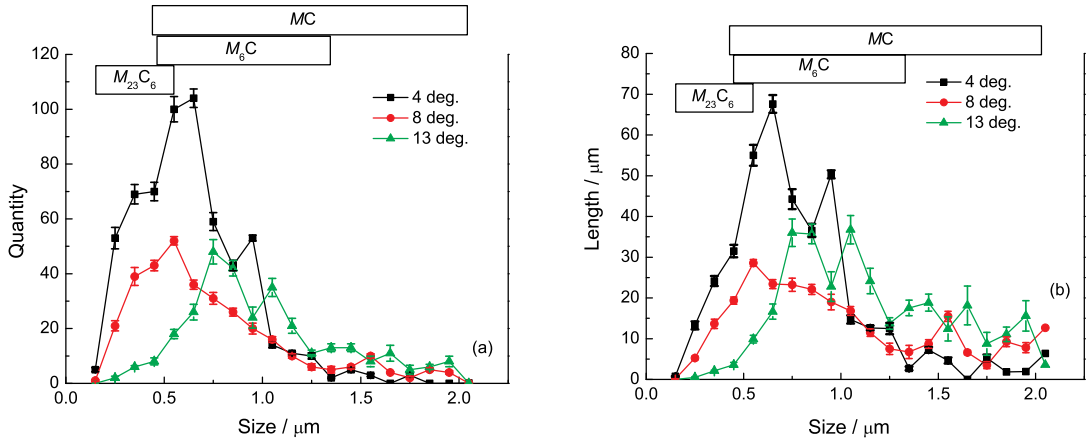

Fig. 3 (a) Size distribution of carbides at grain boundaries in the bicrystal specimens with 4°, 8° and 13° grain boundaries, respectively; (b) total intercept of grain boundary through carbides with different sizes. The measured length for each grain boundary is 650 μm. Black frames illustrate the size range of different carbides

a grain boundary in length of about 650 μm in the bicrystal samples with 4°, 8° and 13° grain boundaries, respectively. The larger the carbide, the longer its intercept length with the grain boundary is. It is seen from this figure that the amount of carbides with the size smaller than 0.5 μm decreases significantly with the increase of misorientation angle. For reckoning the influence of different kinds of carbides with different sizes, we have also measured the total intercept length for each kind of carbides as the total intercept length is determined by both the amount of each kind of carbides and their sizes along the grain boundary. As shown in Fig. 3(b), the total intercept length of carbides with the size larger than 1.3 μm increases with the increase of misorientation angle.

Fig. 4 illustrates the stress rupture lives of the bicrystal superalloys at 800 °C and 750 MPa for grain boundaries with different misorientation angles. From the low to medium angle misorientation, the stress rupture life of bicrystals firstly descends gradually and then sharply falls down to nearly zero just when the angle approaching 13° as shown in Fig. 4.

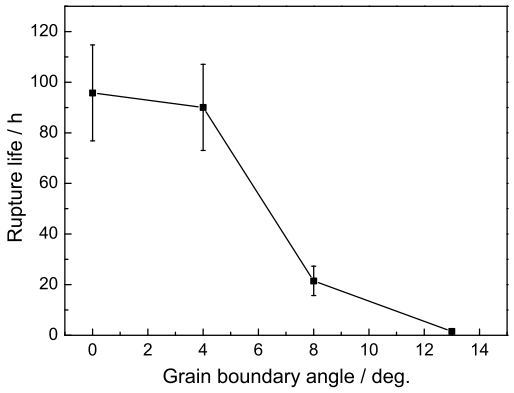

Fig. 4 Stress rupture life of bicrystals with different misorientation angles between secondary dendrites tested at 800 °C and 750 MPa

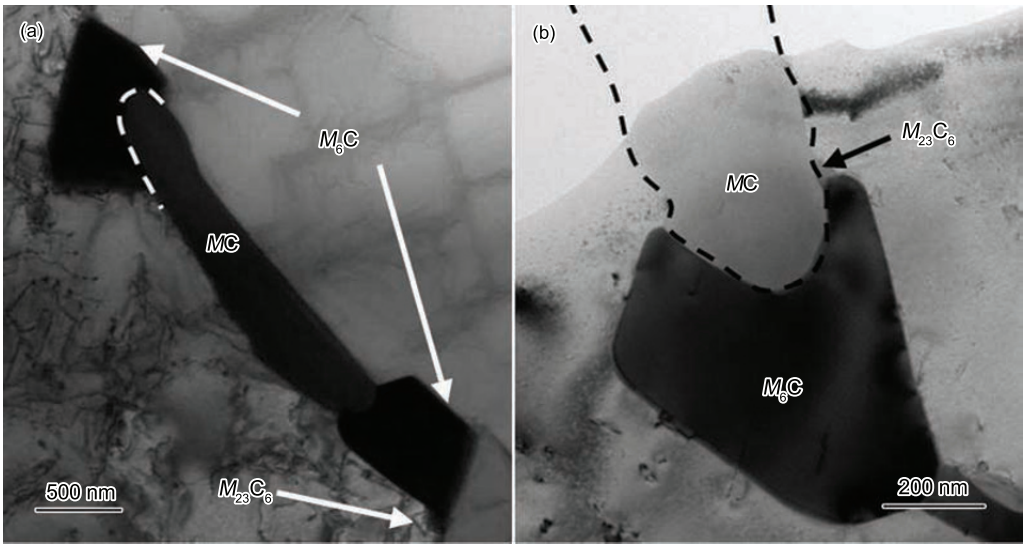

Fig. 5 MC carbides decorated by discrete M_6C and $M_{23}C_6$ particles: (a) $M_{23}C_6$ located on the tip of a M_6C carbide, (b) $M_{23}C_6$ located near MC and M_6C carbides

This tendency is similar to the result obtained for the SRR2072 bicrystal superalloy under the loading condition of 950 °C/210 MPa[3].

3.2 MC carbides at grain boundaries

A large proportion of MC carbides are decorated by discrete M_6C and $M_{23}C_6$ particles as shown in Fig. 5. The MC carbides have high concentration of Ti, Ta but small amount of W (Table 2). Their Cr, Co, Ni concentrations, however, are significantly lower than those in γ and γ' phases. Among the finer particles surrounding the MC carbides, $M_{23}C_6$ particles were frequently observed around or inside the relatively larger M_6C particles (*e.g.* Figs. 5 and 6(g)). Fig. 7 shows the average chemical compositions of the matrix and the vicinity of MC carbides, each of which is the average of 15 measured values by EDS. Comparing with the average composition of the matrix, the vicinity of MC is rich with Cr (about 31 at.%), which is an important $M_{23}C_6$ forming element and W (11 at.%), a M_6C forming element. Fig. 8(b) illustrates the distribution of main elements along a scan line across a decorating M_6C particle shown in Fig. 8(a). It suggests that Cr is easily segregated at certain segments of the M_6C-matrix interfaces. Quantitative analysis indicates a ~47 at.% of Cr concentration in the segregation region less than in the $M_{23}C_6$ phase but significantly higher than in the γ and γ' phases. EDS analysis (Figs. 7 and 8) reveals that there is a local fluctuation of composition around MC and M_6C carbides. As a result, at the location with higher Cr segregation, the formation of $M_{23}C_6$ would be easier.

ORs between the MC carbides along the grain boundaries and matrix were determined by electron diffraction. 20 MC carbides were investigated in specimens of 4° and 8° grain boundaries and their ORs are summarized as follows:

(a) $\{001\}_{\text{carbide}}$// $\{001\}_{\text{matrix}}$, $<100>_{\text{carbide}}$//$<100>_{\text{matrix}}$,
(b) $[001]_{MC}$ // $[310]_{\text{matrix}}$, $(020)_{MC}$//$(1\text{–}31)_{\text{matrix}}$,
(c) $[110]_{MC}$ // $[310]_{\text{matrix}}$, $(\text{–}11\text{–}1)_{MC}$//$(002)_{\text{matrix}}$,
(d) $[001]_{MC}$ // $[001]_{\text{matrix}}$, $(\text{–}260)_{MC}$//$(020)_{\text{matrix}}$.

Table 3 Frequency of observation of various ORs between 20 MC carbides and the matrix. Here, N.A. stands for not applied

OR	(a)	(b)	(c)	(d)	N.A.
Number	9	2	3	3	3

Table 3 lists the experimentally observed frequency to each OR, and the ORs are shown in Fig. 6. It is possible for an OR to display different composite diffraction patterns when viewed in different directions. In order to remove this ambiguity, the composite stereographic projections for the four ORs were plotted in Fig. 9. In each stereographic projection map, the paralleled and near paralleled orientations were shown. As shown in Fig. 9, each OR is different from the other ORs, this suggests that the four ORs are independent. OR (a) is simply cube-cube OR, and was reported for carbides in previous work[2,9–11]. The cube-cube OR between isolated M_6C and $M_{23}C_6$ precipitates and matrix were also found (Fig. 10).

4. Discussion

4.1 Effects of carbide microstructures on stress rupture lives of superalloys

In the present superalloys, the most of carbides

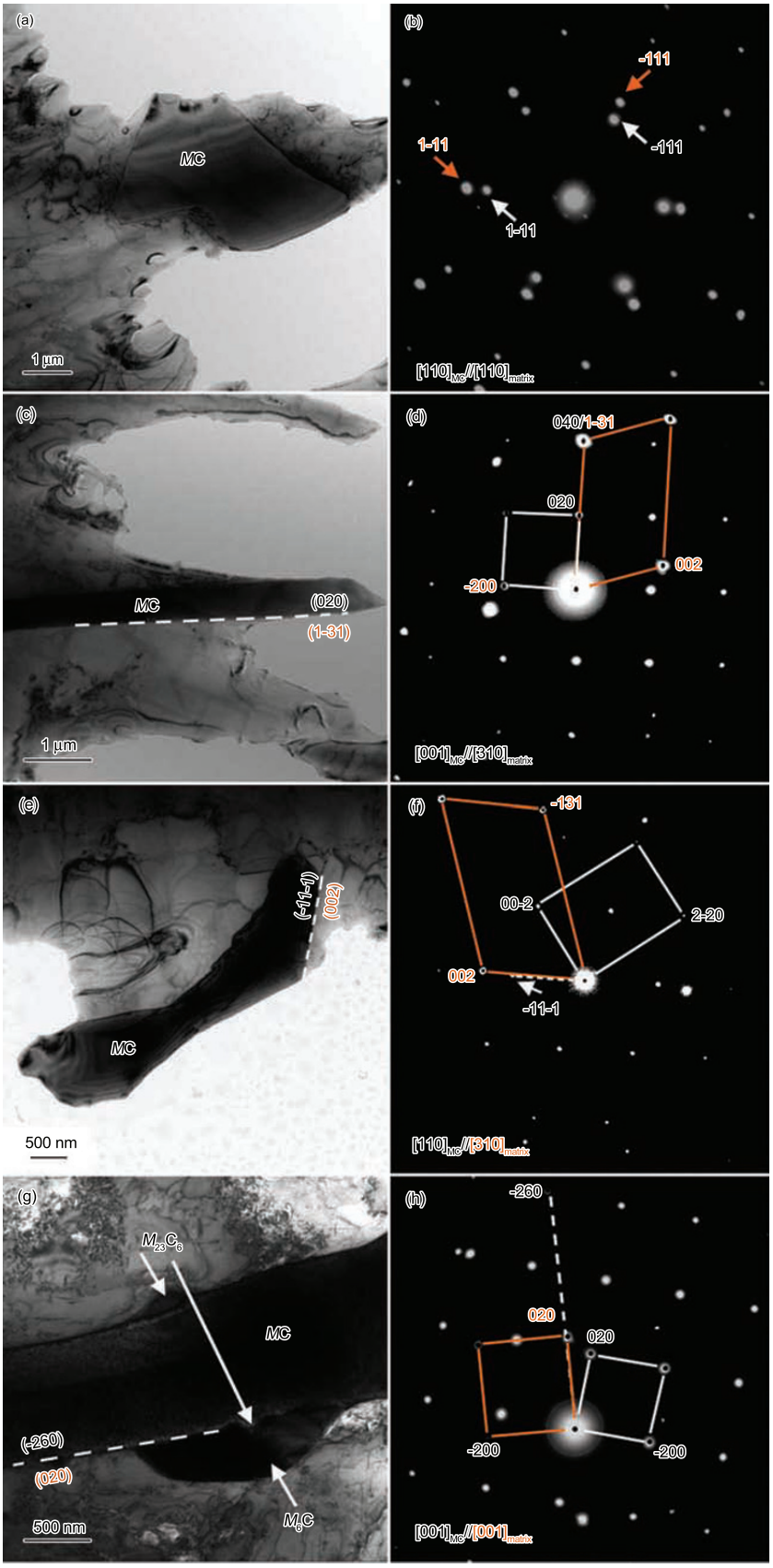

Fig. 6 Bright-field images (a, c, e, g) and corresponding electron diffraction patterns (b, d, f, h) obtained from (b) $[110]_{MC}$ and $[110]_{\gamma/\gamma'}$; (d) $[001]_{MC}$ and $[310]_{\gamma/\gamma'}$, (f) $[110]_{MC}$ and $[310]_{\gamma/\gamma'}$, (h) $[001]_{MC}$ and $[001]_{\gamma/\gamma'}$. In (g), a $M_{23}C_6$ particle locates in a M_6C carbide, where the blurred $M_{23}C_6/M_6C$ interfaces result from the projection of inclined interfaces between $M_{23}C_6$ and M_6C

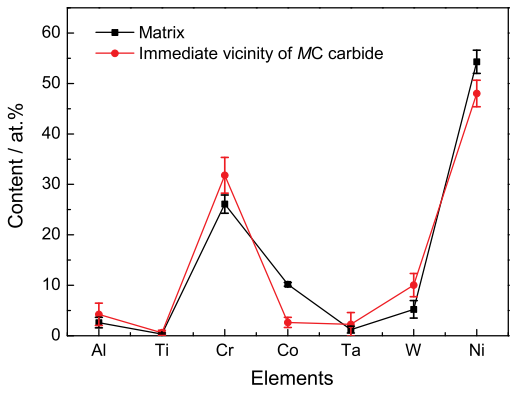

Fig. 7 Average chemical compositions of the matrix and the immediate vicinity of MC carbides

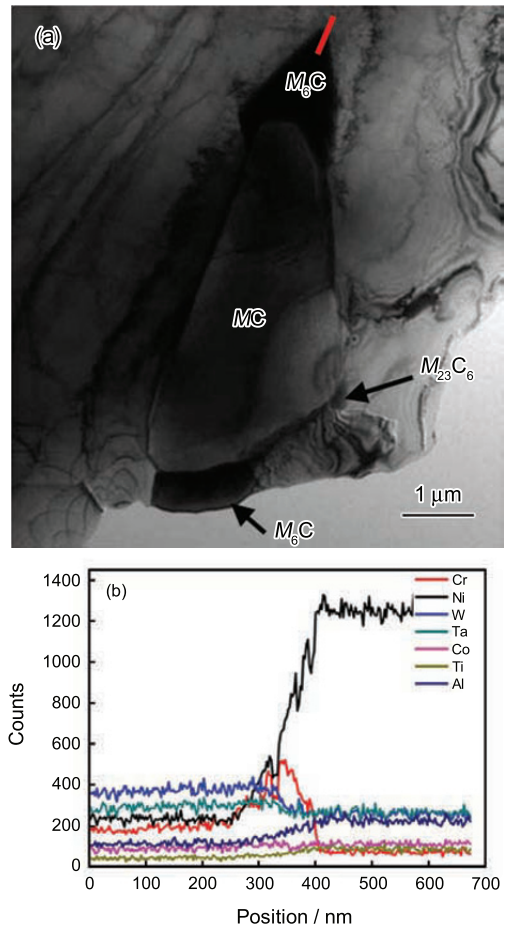

Fig. 8 (a) Bright-field image of carbides and the matrix, (b) EDS line-scan profiles scanned respectively along the red line in (a)

with size smaller than 0.5 μm are $M_{23}C_6$, the carbides with size larger than 1.3 μm are mainly MC, as shown in Fig. 3. From Fig. 3(a), it could be concluded that among all the bicrystal samples, the 4° grain boundary contains the highest density of $M_{23}C_6$ particles at this grain boundary, while the 13° grain boundary contains the lowest density of $M_{23}C_6$ particles. Fig. 3(b) shows that the intercept lengths of MC particles with grain boundary is longer along the 13° grain boundary, while it is shorter along the 4° grain boundary. Correspondingly, the sample of 4° grain boundary exhibits the best stress rupture resistance among all the bicrystals. However the rupture resistance reduces to nearly zero for the sample with 13° grain boundary. This suggests that $M_{23}C_6$ carbides with size smaller than 0.5 μm are evidently beneficial to the stress rupture lives of bicrystals, compared with harmful effects of large MC carbides at grain boundaries.

4.2 Carbide formation at grain boundaries

The formation of $M_{23}C_6$ and M_6C particles in the vicinity of MC carbides is discussed in the following. In general, MC carbides form at the later stage of solidification. This would cause local segregation of Cr and W and the composition fluctuation in the vicinity of these MC carbides would promote the formation of $M_{23}C_6$ and M_6C, especially at the phase boundaries between MC carbides and matrix. With the chemical composition variation in the vicinity of MC carbides at the grain boundaries, $M_{23}C_6$ forms firstly at a higher Cr/W ratio; then M_6C forms at a lower Cr/W ratio. This is why an initially formed $M_{23}C_6$ particle is often surrounded by a M_6C carbide as shown in Fig. 6(g). The relative position of a $M_{23}C_6$ particle to a larger M_6C carbide has been determined by TEM observations with series tilting of specimen. EDS analysis (Fig. 8(b)) revealed that there exists Cr segregation at the tip of a larger M_6C particle. When the TEM specimen was titled around different axes, no significant diffraction contrast was seen near the tip of the M_6C carbide in bright-field images. This means no $M_{23}C_6$ particle exists at the tip of M_6C carbide and in other words the high Cr concentration here is not caused by the existence of $M_{23}C_6$. Therefore, it suggests that the formation of $M_{23}C_6$ at tips of M_6C particles is also attributed to local gradual accumulation of Cr. Besides Cr expelled due to the growth of MC carbides, this accumulation of Cr might come from γ' precipitation process in matrix.

4.3 Interfaces between MC carbides and matrix

Until now, to our best knowledge, ORs (b-d) have not been reported before, however, they were observed in considerable frequencies in this work (Table 3), and this is in contrast to general observations[12,13] that MC carbides exhibit no preferred ORs to matrix except for the occasional cube-cube OR. Furthermore, in ORs (b-d), large and straight segments of MC/matrix interfaces were often observed along the paralleled lattice planes of MC particles and matrix (Fig. 6). The occurrence of these interface planes between MC and matrix agrees with the criterion proposed by Wolf[14] for interfacial energy, where the physical parameter governing interfacial energy is the spacing, $d(hkl)$, of

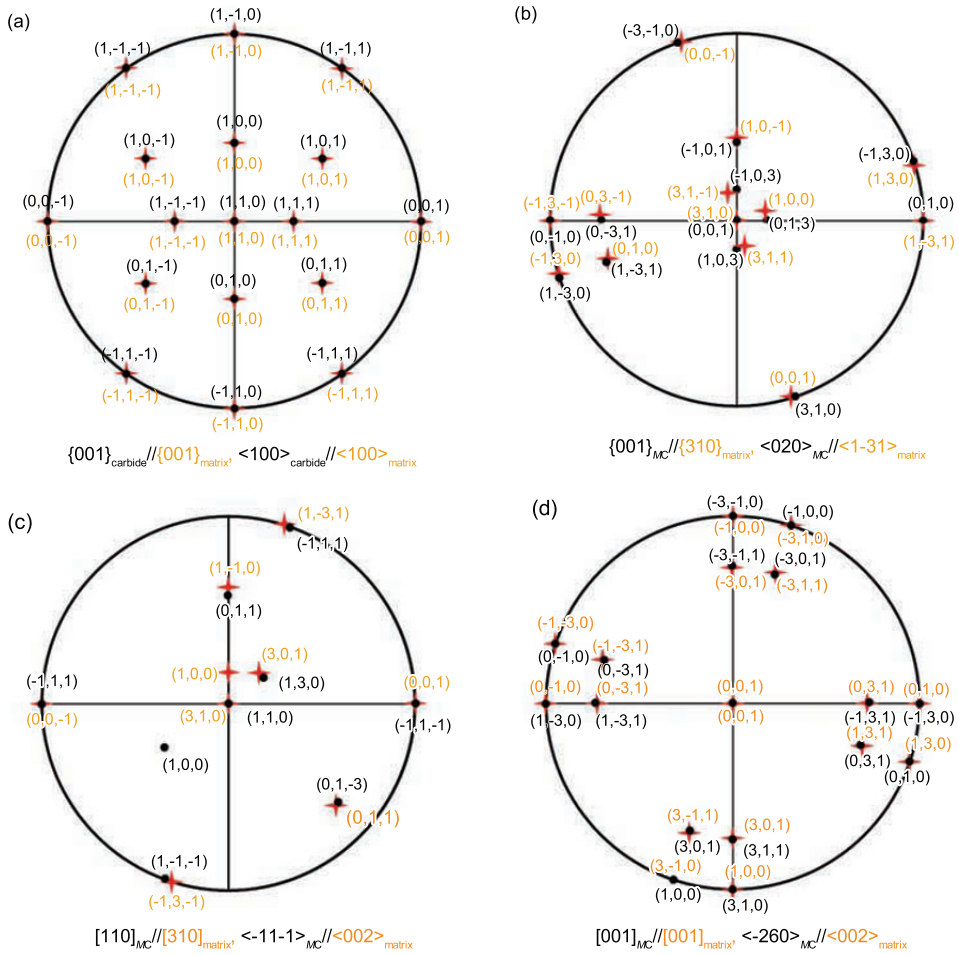

Fig. 9 Composite stereographic projections for the four ORs in Fig. 6: the red stars representing the lattice planes or orientations of matrix, the black spheres representing the lattice planes or orientations of MC

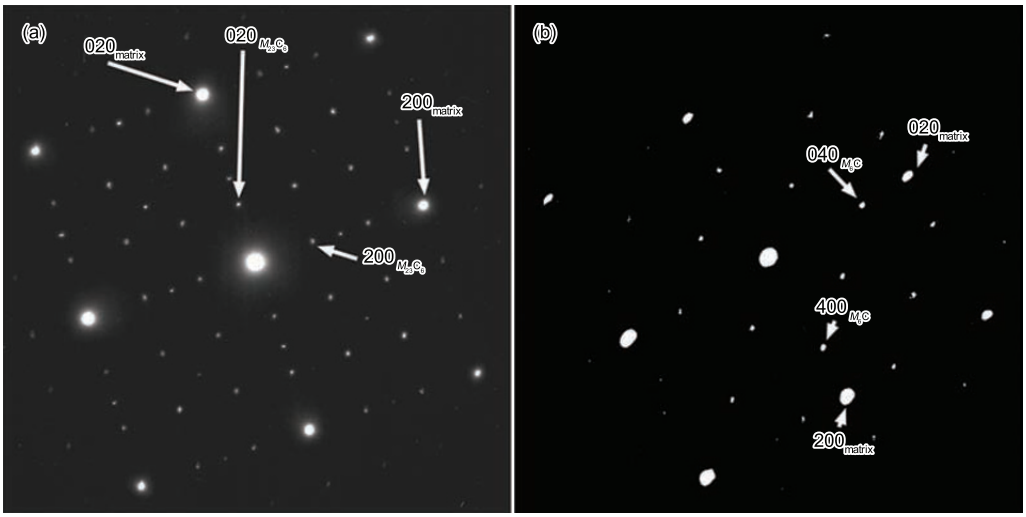

Fig. 10 Cube-cube OR between carbides and the γ/γ' matrix: (a) between $M_{23}C_6$ and γ/γ', along the [001] axis; (b) between M_6C and γ/γ', along the [001] axis

lattice planes (hkl) parallel to the interface plane. It is outlined that $d(hkl)$ represents the closest possible distance between any two atoms facing each other across the interface, and this closest distance between atoms on the two sides of interface contributes the most of interfacial energy. Therefore, when $d(hkl)$

increases, the interfacial energy would decrease significantly. For the observed interfaces in this work, the {020},{311} and {111} planes correspond to the largest $d(hkl)'$s in the face-centered-cubic structured MC and matrix lattices. Therefore, these interfaces are likely to have low interfacial energies. Although as pointed out by Sutton and Balluffi[15] that geometric criteria should not be used generally to predict interfacial energies, this geometric criterion seems just as applicable to our experimental results for the relatively simple interface system of MC/matrix.

5. Conclusions

For the superalloy with 0.015 wt% C, $M_{23}C_6$ carbides with the size smaller than 0.5 μm at grain boundaries demonstrate evidently a beneficial effect on stress rupture lives, but large MC carbides may have an adverse effect.

The local gradual accumulation of Cr and W promotes $M_{23}C_6$ and M_6C formation in the vicinity of MC carbides at grain boundaries in nickel based superalloys. The formation of $M_{23}C_6$ at tips of M_6C particles is also attributed to the local fluctuation of Cr.

A variety of orientation relationships have been observed between MC carbides and the matrix.

Acknowledgements

The authors thank the National Natural Science Foundation of China (Nos. 50671109, 51171188, 50921004 and U1037601) and the Hundred Talents Project of the Chinese Academy of Sciences for financial support.

REFERENCES

[1] T.M. Pollock, R.D. Kissinger, R.R. Bowman, K.A. Green, M. Mclean, S. Olean and J.J. Schirra (Eds.): *Superalloys 2000*, TMS, Warrendale, 2000, 3.

[2] X.Z. Qin, J.T. Guo, C. Yuan, C.L. Chen, J.S. Hou and H.Q. Ye: *Mater. Sci. Eng. A*, 2008, **485**, 74.

[3] Q.Z. Chen, C.N. Jones and D.M. Knowles: *Mater. Sci. Eng. A*, 2004, **385**, 402.

[4] L.Z. He, Q. Zheng, X.F. Sun, H.R. Guan, Z.Q. Hu, A.K. Tieu, C. Lu and H.T. Zhu: *Mater. Sci. Eng. A*, 2005, **397**, 297.

[5] K. Zhao, Y.H. Ma and L.H. Lou: *J. Alloy. Compd.*, 2009, **475**, 648.

[6] L.R. Liu, T. Jin, N.R. Zhao, X.F. Sun, H.R. Guan and Z.Q. Hu: *Mater. Sci. Eng. A* , 2003, **361**, 191.

[7] A.K. Koul and R. Castillo: *Metall. Mater. Trans. A*, 1988, 19, 2049.

[8] Q.Z. Chen, N. Jones and D.M. Knowles: *Acta. Mater.*, 2002, **50**, 1095.

[9] Q.Z. Chen, C.N. Jones and D.M. Knowles: *Scripta Mater.*, 2002, **47**, 669.

[10] L.R. Liu, T. Jin, N.R. Zhao, Z.H. Wang, X.F. Sun, H.R. Guan and Z.Q. Hu: *Mater. Lett.*, 2003, **57**, 4540.

[11] J.X. Yang, Q. Zhang, X.F. Sun, H.R. Guan and Z.Q. Hu: *J. Mater. Sci.*, 2006, **47**, 6476.

[12] G. Lvov, V.I. Levit and M.J. Kaufman: *Metall. Mater. Trans. A*, 2004, **35**, 1669.

[13] E.W. Ross, C.T. Sims, in C.T. Sims, N.S. Stoloff and W.C. Hagel (Eds.): *Superalloys II*, John Wiley & Sons, New York, 1987, 112.

[14] D. Wolf: *J. Phys. Colloques*, 1985, **46**, C4-197.

[15] A.P. Sutton and R.W. Balluffi: *Acta Metall.*, 1987, **35**, 2177.